Mineralogical Magazine, February 2017, Vol. 81(1), pp. 47–60

Lead-antimony sulfosalts from Tuscany (Italy). XVIII. New data on the crystal-chemistry of boscardinite

CRISTIAN BIAGIONI[1,*] AND YVES MOËLO[2]

[1] Dipartimento di Scienze della Terra, Università di Pisa, Via S. Maria 53, I-56126 Pisa, Italy
[2] Institut des Matériaux Jean Rouxel, UMR 6502, CNRS, Université de Nantes, 2, rue de la Houssinière, 44322 Nantes Cedex 3, France

[*Received 27 September 2015; Accepted 1 December 2015; Associate Editor: Anthony Kampf*]

ABSTRACT

Boscardinite, ideally $TlPb_4(Sb_7As_2)_{\Sigma 9}S_{18}$, has been described recently as a new homeotypic derivative of baumhauerite, found at Monte Arsiccio mine, Apuan Alps, Tuscany, Italy. New findings of boscardinite in different mineral associations of this deposit have allowed the collection of new crystal-chemical data. Electron-microprobe analysis of the crystal used for the single-crystal X-ray diffraction study gave (in wt.%): Ag 1.81(5), Tl 12.60(21), Pb 17.99(12), Hg 0.14(5), As 9.36(12), Sb 33.60(27), S 23.41(30), Cl 0.06(1), total 98.97(100). On the basis of $\Sigma Me = 14$ apfu, it corresponds to $Ag_{0.42}Tl_{1.52}Pb_{2.14}Hg_{0.02}(Sb_{6.82}As_{3.08})_{\Sigma 9.90}S_{18.04}Cl_{0.04}$. With respect to the type specimen, these new findings are characterized by a strong Pb depletion, coupled with higher Tl contents, and a significant As enrichment. The single-crystal X-ray diffraction study of this (Tl,As)-enriched boscardinite confirms the structural features described for the type sample. The unit-cell parameters are $a = 8.1017(4)$, $b = 8.6597(4)$, $c = 22.5574(10)$ Å, $\alpha = 90.666(2)$, $\beta = 97.242(2)$, $\gamma = 90.850(2)°$, $V = 1569.63(12)$ Å^3, space group $P\bar{1}$. The crystal structure was refined down to $R_1 = 0.0285$ on the basis of 6582 reflections with $F_o > 4\sigma(F_o)$. Arsenic is dominant in three MeS_3 sites, compared to one in type boscardinite. The main As-enrichment is observed in the sartorite-type sub-layer. Owing to this chemical peculiarity, (Tl,As)-rich boscardinite shows alternation, along **b**, of Sb-rich sites and As-rich sites; this feature represents the main factor controlling the 8 Å superstructure. The chemical variability of boscardinite is discussed; the Ag increase observed here gets closer to stoichiometric $AgTl_3Pb_4(Sb_{14}As_6)_{\Sigma 20}S_{36}$ ($Z = 1$), against possible extension up to $AgTl_2Pb_6(Sb_{15}As_4)_{\Sigma 19}S_{36}$ for type boscardinite.

KEYWORDS: boscardinite, sartorite homologous series, thallium, silver, sulfosalt, Monte Arsiccio mine, Apuan Alps, Tuscany, Italy

Introduction

BOSCARDINITE, ideally $TlPb_4(Sb_7As_2)_{\Sigma 9}S_{18}$, is an N = 3.5 member of the sartorite homologous series (Makovicky, 1985). It is the (Tl,Sb)-homeotype of baumhauerite, first described by Orlandi *et al*. (2012) from the Sant'Olga level, Monte Arsiccio mine, Apuan Alps, Tuscany, Italy. In the type material boscardinite occurs as mm-sized lead grey compact metallic masses embedded in a quartz vein, in association with zinkenite. A second occurrence of boscardinite has been described by Topa *et al*. (2013) in intimate intergrowth with stibnite and smithite from the Jas Roux thallium mineralization, Hautes-Alpes, France.

After the first finding of boscardinite in a quartz vein (occurrence of Type 3 in agreement with Biagioni *et al*., 2014*b*) embedded in the dolostone from the Sant'Olga level, new specimens of boscardinite-like sulfosalts have been found in the microcrystalline baryte + pyrite ore bodies, at the contact between schist and dolostone (Type 1 occurrence), and in the pyrite-rich dolostone (Type 2 occurrence). In particular, in this latter kind of occurrence, boscardinite is

*E-mail: biagioni@dst.unipi.it
https://doi.org/10.1180/minmag.2016.080.068

TABLE 1. Microprobe analyses of (Tl,As)-enriched boscardinite: chemical composition as wt.% and chemical formula (in atoms per formula unit, apfu) on the basis of Σ*Me* = 14 apfu.

	Sant'Olga (sample #408)			Sant'Anna (sample #2)		
Element	wt.%	Range (n = 3)	e.s.d.	wt.%	Range (n = 3)	e.s.d.
Ag	1.81	1.77–1.87	0.05	1.46	1.42–1.51	0.05
Tl	12.60	12.39–12.82	0.21	11.38	11.33–11.43	0.05
Pb	17.99	17.85–18.09	0.12	20.57	20.46–20.79	0.19
Hg	0.14	0.10–0.20	0.05	0.13	0.10–0.16	0.03
As	9.36	9.23–9.46	0.12	8.24	8.22–8.24	0.01
Sb	33.60	33.28–33.77	0.27	33.48	33.39–33.55	0.08
S	23.41	23.09–23.70	0.30	22.89	22.81–22.96	0.07
Cl	0.06	0.05–0.07	0.01	0.05	0.03–0.08	0.03
sum	98.97	97.82–99.56	1.00	98.20	98.15–98.27	0.06
apfu						
Ag	0.42	0.40–0.43	0.01	0.34	0.33–0.35	0.01
Tl	1.52	1.51–1.54	0.01	1.41	1.40–1.42	0.01
Pb	2.14	2.14–2.15	0.01	2.51	2.50–2.53	0.02
Hg	0.02	0.01–0.02	0.01	0.02	0.01–0.02	0.00
As	3.08	3.07–3.10	0.01	2.78	2.77–2.78	0.00
Sb	6.82	6.81–6.83	0.01	6.95	6.94–6.97	0.02
S	18.04	17.96–18.16	0.11	18.04	17.96–18.11	0.08
Cl	0.04	0.04–0.05	0.00	0.04	0.02–0.06	0.02
Ev (%)*	–0.4	–1.1 to –0.1	0.6	–0.4	–0.9 to 0.1	0.5

*Relative error on the valence equilibrium (%), calculated as [Σ(val+) – Σ(val–)] × 100 / Σ(val–).

associated with protochabournéite and routhierite, forming compact black masses up to 1 cm in size. The chemical characterization of these new specimens of boscardinite revealed some peculiarities, in particular, a strong Pb depletion, coupled with higher Tl contents, and a significant As enrichment. Consequently, a structural study was performed.

A similar chemistry was observed in an additional specimen of boscardinite collected in the Sant'Anna level, an upper underground level of the Monte Arsiccio mine. In this further specimen, boscardinite occurs in thin veinlets within a grey dolostone, intimately associated with a 'protochabournéite-like' mineral and small red grains of cinnabar.

The aim of this paper is to contribute to the knowledge of the crystal chemistry of sartorite homologues and, in particular, of the (Tl,Sb)-homeotypic derivative of baumhauerite.

Experimental

Chemical analysis

Two specimens of boscardinite from the Sant'Olga (sample #408) and the Sant'Anna levels (sample #2) were analysed with a CAMEBAX SX100 electron microprobe. The operating conditions were: accelerating voltage 20 kV, beam current 20 nA, beam size 1 μm. Standards (element, emission line, counting times for one spot analysis) are: galena (Pb, *Mα*, 60 s), stibnite (Sb, *Lα*, 60 s), AsGa (As, *Lα*, 30 s), pyrite (S, *Kα*, 60 s), Ag (Ag, *Lα*, 30 s), lorándite (Tl, *Mα*, 20 s), cinnabar (Hg, *Mα*, 20 s) and pyromorphite (Cl, *Kα*, 30 s). Results are given in Table 1. On the basis of Σ*Me* = 14 atoms per formula unit (apfu), the corresponding chemical formulae are $Ag_{0.42}Tl_{1.52}Hg_{0.02}Pb_{2.14}(Sb_{6.82}As_{3.08})_{\Sigma 9.90}S_{18.04}Cl_{0.04}$ and $Ag_{0.34}Tl_{1.41}Hg_{0.02}Pb_{2.51}(Sb_{6.95}As_{2.78})_{\Sigma 9.73}S_{18.04}Cl_{0.04}$ for samples #408 and #2, respectively. Each of the two groups of analytical data is very homogeneous. The $As/(As + Sb)_{at.}$ ratio is 0.31 and 0.29 for samples #408 and #2, respectively, to be compared with the values 0.21 and 0.24 for samples #4977 and #4989 described by Orlandi *et al.* (2012). Moreover, the $Pb/(Pb + 2Tl)_{at.}$ ratios are 0.41 (#408) and 0.47 (#2), to be compared with 0.54 (#4977) and 0.59 (#4989). Thus, the new specimens of boscardinite are richer in Tl and As than type boscardinite.

Applying the substitutions $Hg^{2+} + Pb^{2+} = Ag^{+} + Sb^{3+}$, $Ag^{+} + Sb^{3+} = 2Pb^{2+}$ and $Pb^{2+} + Cl^{-} = Sb^{3+} +$

https://doi.org/10.1180/minmag.2016.080.068 Published online by Cambridge University Press

TABLE 2. Crystal data and summary of parameters describing data collection and refinement for (Tl,As)-enriched boscardinite.

Crystal data	
Structural formula	$Ag_{0.40}Tl_{1.51}Pb_{2.10}(Sb_{7.13}As_{2.86})_{\Sigma 9.99}S_{18}$
Crystal size (mm)	0.10 × 0.10 × 0.05
Cell setting, space group	Triclinic, $P\bar{1}$
a, *b*, *c* (Å)	8.1017(4), 8.6597(4), 22.5574(10)
α, β, γ (°)	90.666(2), 97.242(2), 90.850(2)
V (Å^3)	1569.63(12)
Z	2
Data collection and refinement	
Radiation, wavelength (Å)	Mo*K*α, λ = 0.71073
Temperature (K)	293
Maximum observed 2θ (°)	55.31
Measured reflections	26,678
Unique reflections	7211
Reflections $F_o > 4\sigma(F_o)$	6582
R_{int} after absorption correction	0.0195
$R\sigma$	0.0171
Range of *h*, *k*, *l*	$-10 \le h \le 10$, $-11 \le k \le 11$, $-29 \le l \le 29$
R [$F_o > 4\sigma(F_o)$]	0.0285
R (all data)	0.0330
wR (on F_o^2)	0.0707
Goof	1.115
Number of least-squares parameters	314
Maximum and minum residual peak (*e*/Å^3)	2.70 (at 0.73 Å from Pb3a) –3.38 (at 0.67 Å from Sb4b)

S^{2-}, the following formulae can be obtained: $Tl_{1.52}Pb_{2.96}(Sb_{6.44}As_{3.08})_{\Sigma 9.52}S_{18.08}$ (sample #408) and $Tl_{1.41}Pb_{3.17}(Sb_{6.65}As_{2.78})_{\Sigma 9.43}S_{18.08}$ (sample #2). They are close to the simplified formula $Tl_{1.5}Pb_3(Sb_{6.5}As_3)_{\Sigma 9.5}S_{18}$.

Single-crystal X-ray diffraction

The sample #408, being the richest in Tl and As between the two new samples studied, was used for the single-crystal X-ray diffraction study. Intensity data were collected using a Bruker Smart Breeze diffractometer equipped with an air-cooled CCD detector, with Mo*K*α radiation. The detector-to-crystal distance was 60 mm. 4896 frames were collected using ω and φ scan modes, in 0.25° slices, with an exposure time of 45 s per frame. The data were corrected for the Lorentz and polarization factors and absorption using the software package *Apex2* (Bruker AXS Inc., 2004*b*). The statistical tests on the distribution of |*E*| values ($|E^2 - 1|$ = 0.981) and the systematic absences are consistent with the space group $P\bar{1}$. The refined unit-cell parameters are *a* = 8.1017(4), *b* = 8.6597(4), *c* = 22.5574(10) Å, α = 90.666(2), β = 97.242(2), γ = 90.850(2)°, *V* = 1569.63(12) Å^3.

The crystal structure was refined using *Shelxl-97* (Sheldrick, 2008) starting from the atomic coordinates of boscardinite given by Orlandi *et al*. (2012). Scattering curves for neutral atoms were taken from the *International Tables for Crystallography* (Wilson, 1992). Crystal data and details of the intensity data collection and refinement are reported in Table 2. The site-occupation factor (s.o.f.) of mixed (Sb/As) and (Sb/Ag) sites was refined freely using the scattering curves of Sb *vs.* As and Sb *vs.* Ag, respectively. On the contrary, the s.o.f. of mixed (Tl/Pb) sites was fixed on the basis of bond-valence calculations, owing to the similarity between the site-scattering values of Tl and Pb. After several cycles of isotropic refinement, the R_1 converged to 0.097, thus confirming the correctness of the structural model. The isotropic displacement parameter at the Pb3 and Pb4 sites proved to be relatively high, suggesting the replacement of (Pb,Tl) by a lighter atom, i.e. Sb. The s.o.f. of these two sites was refined using the scattering curves Pb *vs.* Sb, freely refining

https://doi.org/10.1180/minmag.2016.080.068 Published online by Cambridge University Press

their coordinates; the R_1 factor lowered to 0.077. Introducing the anisotropic displacement parameters for all cation positions made the refinement converge to $R_1 = 0.038$. Finally, an anisotropic model for all the atom positions lowered the final R_1 value to 0.028 for 6582 reflections with $F_o > 4\sigma(F_o)$ and 0.033 for all 7211 independent reflections. The highest and deepest residuals are located around Pb3a and Sb4b sites, respectively. Atomic coordinates and selected bond distances are reported in Table 3 and Table 4, respectively. Bond-valence sums (BVS) are given in Table 5.

Crystal structure of (Tl,As)-enriched boscardinite

General features, cation coordination and site occupancies

The general organization of the crystal structure fully agrees with that described by Orlandi *et al.* (2012) for boscardinite (Fig. 1). This mineral, belonging to the sartorite homologous series, is formed by the 1:1 alternation, along **c**, of a sartorite-type layer (N = 3) and a dufrénoysite-type layer (N = 4), connected by zig-zag chains of (Pb,Tl,Sb) atoms running along

TABLE 3. Atomic positions and equivalent isotropic displacement parameters (in Å^2) for (Tl,As)-enriched boscardinite.

Site	Occupancy	*x/a*	*y/b*	*z/c*	U_{eq}
Tl1	$Tl_{0.90}Pb_{0.10}$	0.12401(5)	0.63926(4)	0.17007(1)	0.0407(1)
Tl2a	$Tl_{0.23}Pb_{0.18}$	0.8661(5)	0.8796(4)	0.8247(2)	0.0446(4)
Tl2b	$Tl_{0.38}Pb_{0.21}$	0.8339(3)	0.8481(2)	0.8293(1)	0.0446(4)
Pb3a	$Pb_{0.757(5)}$	0.6717(2)	0.6538(3)	0.2605(1)	0.0423(3)
Sb3b	$Sb_{0.243(5)}$	0.6977(15)	0.653(2)	0.2589(8)	0.0423(3)
Pb4a	$Pb_{0.811(5)}$	0.66469(10)	0.14674(11)	0.25837(4)	0.0427(2)
Sb4b	$Sb_{0.189(5)}$	0.6654(10)	0.1672(9)	0.2435(3)	0.0427(2)
Sb1	$Sb_{1.00}$	0.55493(6)	0.39577(6)	0.10135(2)	0.0256(1)
Sb2	$Sb_{1.00}$	0.82275(6)	0.10871(5)	0.01945(2)	0.0231(1)
As3	$As_{0.60(1)}Sb_{0.40(1)}$	0.46832(8)	0.11462(7)	0.88187(3)	0.0280(2)
As4	$As_{0.87(1)}Sb_{0.13(1)}$	0.18682(8)	0.36301(8)	0.00280(3)	0.0240(2)
Sb5	$Sb_{0.51(1)}As_{0.49(1)}$	0.07572(7)	0.39082(7)	0.33278(3)	0.0280(2)
Sb6	$Sb_{0.73(1)}As_{0.27(1)}$	0.11230(7)	0.85087(7)	0.34549(2)	0.0312(2)
Sb7	$Sb_{1.00}$	0.84624(6)	0.34108(6)	0.46601(2)	0.0327(1)
As8	$As_{0.63(1)}Sb_{0.37(1)}$	0.79017(8)	0.90055(8)	0.44478(3)	0.0344(2)
Sb9a	$Sb_{0.956(3)}$	0.43016(14)	0.15697(12)	0.41082(3)	0.0327(2)
Pb9b	$Pb_{0.044(3)}$	0.382(2)	0.1197(14)	0.4157(5)	0.0327(2)
Sb10a	$Sb_{0.60(1)}$	0.4774(4)	0.6011(4)	0.4285(2)	0.0472(6)
Ag10b	$Ag_{0.40(1)}$	0.4708(7)	0.6340(6)	0.4138(3)	0.0472(6)
S1	$S_{1.00}$	0.3622(2)	0.1791(2)	0.04453(10)	0.0336(4)
S2	$S_{1.00}$	0.9243(2)	0.6928(2)	0.39903(9)	0.0286(4)
S3	$S_{1.00}$	0.2737(2)	0.9117(2)	0.85895(7)	0.0235(3)
S4	$S_{1.00}$	0.9092(2)	0.3927(2)	0.23876(9)	0.0342(4)
S5	$S_{1.00}$	0.6267(2)	0.3579(2)	0.37759(8)	0.0261(3)
S6	$S_{1.00}$	0.6707(2)	0.1684(2)	0.51583(8)	0.0270(4)
S7	$S_{1.00}$	0.9918(2)	0.0921(2)	0.93289(7)	0.0212(3)
S8	$S_{1.00}$	0.9297(2)	0.8801(2)	0.25565(8)	0.0273(4)
S9	$S_{1.00}$	0.3328(2)	0.5684(2)	0.05246(8)	0.0247(3)
S10	$S_{1.00}$	0.2959(2)	0.4240(2)	0.47268(10)	0.0322(4)
S11	$S_{1.00}$	0.9699(3)	0.0885(2)	0.41704(11)	0.0377(5)
S12	$S_{1.00}$	0.9850(2)	0.3412(2)	0.06757(8)	0.0241(3)
S13	$S_{1.00}$	0.5736(2)	0.9272(3)	0.36456(9)	0.0359(4)
S14	$S_{1.00}$	0.2555(2)	0.1942(2)	0.30754(8)	0.0314(4)
S15	$S_{1.00}$	0.7096(2)	0.6768(2)	0.14139(8)	0.0249(3)
S16	$S_{1.00}$	0.2547(2)	0.6023(2)	0.31409(9)	0.0299(4)
S17	$S_{1.00}$	0.4410(2)	0.3767(2)	0.19628(8)	0.0281(4)
S18	$S_{1.00}$	0.5775(3)	0.1029(2)	0.79103(9)	0.0352(4)

https://doi.org/10.1180/minmag.2016.080.068 Published online by Cambridge University Press

TABLE 4. Selected bond distances (in Å) for (Tl,As)-enriched boscardinite.

Tl1–S4	3.261(2)	Tl2a–S14	3.078(5)	Tl2b–S17	2.933(3)	Pb3a–S15	2.751(3)
–S18	3.296(2)	S18	3.083(5)	–S12	3.090(3)	–S8	2.857(3)
–S16	3.308(2)	–S7	3.097(4)	–S14	3.096(3)	–S4	3.065(3)
–S15	3.360(2)	–S12	3.233(4)	–S18	3.108(4)	–S18	3.076(3)
–S8	3.365(2)	–S17	3.295(3)	–S7	3.258(3)	–S17	3.233(3)
–S7	3.366(2)	–S3	3.302(4)	–S1	3.438(4)	–S13	3.485(3)
–S9	3.376(2)	–S8	3.331(4)	–S4	3.449(4)	–S2	3.523(3)
–S17	3.455(2)	–S4	3.410(5)	–S3	3.575(3)	–S5	3.748(3)
–S12	3.520(2)	–S1	3.709(5)	–S8	3.712(3)	–S16	3.751(3)
Sb3b–S15	2.68(2)	Pb4a–S3	2.796(2)	Sb4b–S3	2.512(7)	Sb1–S17	2.442(2)
–S8	2.71(2)	–S17	2.957(2)	–S17	2.718(9)	–S9	2.512(2)
–S4	2.92(2)	–S4	2.962(2)	–S4	2.770(8)	–S1	2.638(2)
–S18	3.21(2)	–S18	3.005(2)	–S18	3.063(8)	–S15	2.808(2)
–S17	3.33(2)	–S8	3.182(2)	–S8	3.297(9)	–S3	3.110(2)
–S2	3.46(2)	–S13	3.226(2)	–S5	3.481(7)	–S12	3.696(2)
–S13	3.59(2)	–S5	3.284(2)	–S13	3.595(8)	–S9	3.711(2)
		–S14	3.653(2)				
Sb2–S7	2.480(2)			As4–S1	2.282(2)	Sb5–S4	2.366(2)
–S7	2.527(2)	As3–S18	2.334(2)	–S9	2.319(2)	–S14	2.368(2)
–S12	2.544(2)	–S15	2.350(2)	–S12	2.333(2)	–S16	2.393(2)
–S3	2.952(2)	–S3	2.352(2)	–S7	3.108(2)	–S2	3.323(2)
–S1	3.130(2)	–S1	3.277(2)	–S12	3.265(2)	–S11	3.415(2)
–S9	3.425(2)	–S9	3.390(2)	–S15	3.474(2)	–S10	3.430(2)
Sb6–S8	2.372(2)	Sb7–S6	2.429(2)	As8–S11	2.312(2)	Sb9a–S5	2.525(2)
–S2	2.468(2)	–S5	2.506(2)	–S13	2.372(2)	–S13	2.593(2)
–S16	2.591(2)	–S11	2.701(2)	–S2	2.404(2)	–S14	2.595(2)
–S11	2.938(2)	–S10	2.790(2)	–S6	3.042(2)	–S6	2.871(2)
–S14	3.335(2)	–S2	3.379(2)	–S11	3.459(3)	–S10	2.976(2)
–S6	3.397(2)	–S2	3.502(2)	–S10	3.499(2)	–S6	3.424(2)
		–S10	3.686(2)				
Pb9b–S14	2.616(11)			Ag10b–S16	2.680(7)		
–S13	2.645(10)	Sb10a–S10	2.418(4)	–S6	2.686(6)		
–S6	3.004(14)	–S10	2.717(5)	–S10	2.745(5)		
–S5	3.044(15)	–S6	2.719(4))	–S5	2.878(6)		
–S10	3.047(10)	–S5	2.754(4)	–S13	2.934(5)		
–S6	3.059(11)	–S16	2.957(5)	–S10	3.036(7)		
–S11	3.352(13)	–S13	3.313(5)				

a. Sartorite layers are flanked by Tl sites, hosting minor Pb, whereas the dufrénoysite layer is flanked by mixed and split (Pb/Sb) sites. It should be noted that the sartorite layers in type boscardinite are flanked by alternating (Tl,Pb) and (Pb,Tl) sites, whereas the dufrénoysite layers are flanked by pure Pb and mixed (Pb,Tl) sites.

Within the layers, mixed (Sb/As) sites, with various $(As/Sb)_{at.}$ ratios, occur. Owing to the higher $As/(As + Sb)_{at.}$ ratio with respect to the type boscardinite, pure Sb sites are accompanied by mixed (Sb/As) sites, either Sb- or As-dominant. Within the dufrénoysite-type layer, the alternation along **b** of one (Sb/Pb) site and one (Ag/Sb) site occurs, similar to the configuration observed in rathite (Berlepsch *et al.*, 2002), barikaite (Makovicky and Topa, 2013) and carducciite (Biagioni *et al.*, 2014*c*).

Cation coordinations correspond to those described by Orlandi *et al.* (2012) for type boscardinite. Bond-valence sums (Table 5) are good; the most important deviations are represented by the valence deficit of the Sb atoms at the Sb3b and Sb4b sites, related to the ligand positions that are actually averaged S positions for the (Pb/Sb) mixture at those sites. Table 6 gives a comparison between site occupancies and average bond distances for type boscardinite and its (Tl,As)-enriched analogue. The

https://doi.org/10.1180/minmag.2016.080.068 Published online by Cambridge University Press

TABLE 5. Bond-valence balance (in valence units, vu) in (Tl,As)-enriched boscardinite using the parameters proposed by Brese and O'Keeffe (1991).

	Tl1	Tl2a	Tl2b	Pb3a	Sb3b	Pb4a	Sb4b	Sb1	Sb2	As3a	As4	Sb5	Sb6	Sb7	As8	Sb9a	Pb9b	Sb10a	Ag10b	Σ_{anions}
S1		0.02	0.06					0.60	0.16	0.08	1.02									1.94
S2				0.05	0.02							0.08	0.85	0.08	0.85					1.99
														0.06						
S3		0.06	0.04			0.42	0.16	0.17	0.26	0.99										2.10
S4	0.18	0.05	0.06	0.19	0.07	0.27	0.08					1.01								1.91
S5				0.03		0.11	0.01							0.86		0.78	0.01	0.26	0.06	2.12
S6													0.07	1.06	0.15	0.31	0.01	0.29	0.09	1.97
																0.07	0.01			
S7	0.13	0.11	0.10						0.92		0.11									2.18
									0.81											
S8	0.13	0.06	0.03	0.33	0.12	0.15	0.02						1.10							1.94
S9	0.13							0.85	0.07	0.06	0.93									1.94
								0.03												
S10												0.06		0.40	0.04	0.23	0.01	0.65	0.08	1.84
														0.04				0.29	0.04	
S11												0.06	0.24	0.51	1.08		0.01			1.95
															0.05					
S12	0.09	0.07	0.16					0.03	0.78		0.89									2.09
											0.07									
S13				0.06	0.01	0.13	0.01								0.92	0.65	0.03	0.06	0.05	1.92
S14		0.11	0.16			0.04						1.00	0.08			0.65	0.04			2.08
S15	0.14			0.44	0.13			0.38		0.99	0.04									2.12
S16	0.16			0.03								0.94	0.61					0.15	0.10	1.99
S17	0.11	0.06	0.24	0.12	0.02	0.27	0.09	1.02												1.93
S18	0.16	0.11	0.15	0.18	0.03	0.24	0.04			1.04										1.95
$\Sigma_{cations}$	1.23	0.65	1.00	1.43	0.41	1.63	0.41	3.08	3.00	3.16	3.06	3.15	2.95	3.01	3.09	2.69	0.12	1.70	0.42	
Theor.*	1.10	0.59	0.80	1.51	0.72	1.62	0.57	3.00	3.00	3.00	3.00	3.00	3.00	3.00	3.00	2.87	0.09	1.80	0.40	

*In mixed sites, bond-valence contribution of each cation has been weighted according to its occupancy (see Table 3).

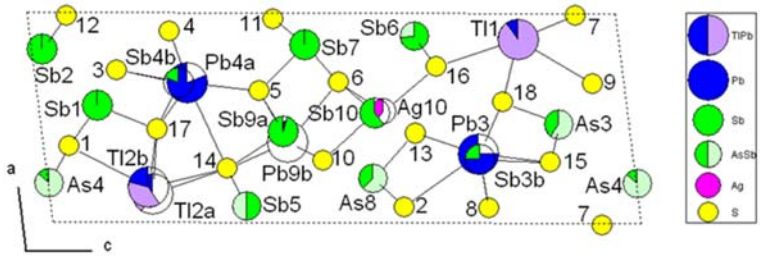

FIG. 1. Crystal structure of (Tl,As)-rich boscardinite as seen down **b**. Numbers without specification refer to S sites.

most remarkable differences involve the cations forming the zig-zag chains of heavy atoms separating the dufrénoysite type layers from the sartorite type ones. In particular, the (Pb,Tl)2a/(Pb,Tl)2b split pair is replaced by two Tl2a and Tl2b split positions dominated by thallium, as shown by the larger average bond distances. This substitution possibly correlates with the occurrence of minor Sb at the Pb3 and Pb4 positions, which are split into two sub-positions (Pb3a/Sb3b) and (Pb4a/Sb4b), respectively. In type boscardinite, these sites have been modelled as a mixed (Pb,Tl)3 and a pure Pb4 site (see below).

Owing to the similar scattering factors for Tl and Pb, their s.o.f. was proposed on the basis of bond-valence calculation, by using, for the pair (Tl,S), the bond-valence parameter $R_{Tl,S}$ tabulated by Brese and O'Keeffe (1991), i.e. 2.63 Å, or alternatively, the value proposed by Biagioni *et al.* (2014*a*), i.e. 2.55 Å. Table 7 shows the s.o.f. of mixed (Tl/Pb) sites on the basis of the two proposed $R_{Tl,S}$ values in type boscardinite and in (Tl,As)-enriched boscardinite. The use of the bond-valence parameter given by Brese and O'Keeffe (1991) results in an underestimation of the Tl content in (Tl,As)-enriched boscardinite ($\Sigma Tl = 1.27$ apfu, to be compared with 1.52 apfu obtained through electron-microprobe analysis). This underestimation does not apparently occur in type boscardinite, possibly owing to the fact that Orlandi *et al.* (2012) interpreted the low BVS at the Pb3 site as due to the occurrence of minor Tl. In (Tl,As)-rich boscardinite, this position is split into two partially occupied Pb

TABLE 6. Site occupancies in type boscardinite (Orlandi *et al.*, 2012) and in (Tl,As)-enriched boscardinite. Site labels agree with those given in Table 3. Average <*Me*–S> distances for (Sb/As) sites have been calculated considering bond distances shorter than 3.0 Å.

	Orlandi *et al.* (2012)		This work	
Site	s.o.f.	<*Me*–S>	s.o.f.	<*Me*–S>
Tl1	$Tl_{0.80}Pb_{0.20}$	3.371	$Tl_{0.90}Pb_{0.10}$	3.367
Tl2a/Tl2b	$Pb_{0.77}Tl_{0.23}$	3.165/3.265	$Tl_{0.61}Pb_{0.39}$	3.282/3.295
Pb3a/Sb3b	$Pb_{0.80}Tl_{0.20}$	3.315	$Pb_{0.76}Sb_{0.24}$	3.276/2.77
Pb4a/Sb4b	$Pb_{1.00}$	3.136	$Pb_{0.81}Sb_{0.19}$	3.133/2.667
Sb1	$Sb_{1.00}$	2.601	$Sb_{1.00}$	2.600
Sb2	$Sb_{1.00}$	2.617	$Sb_{1.00}$	2.626
As3	$Sb_{0.71}As_{0.29}$	2.408	$As_{0.60}Sb_{0.40}$	2.345
As4	$As_{0.75}Sb_{0.25}$	2.334	$As_{0.87}Sb_{0.13}$	2.311
Sb5	$Sb_{0.78}As_{0.22}$	2.415	$Sb_{0.51}As_{0.49}$	2.378
Sb6	$Sb_{1.00}$	2.619	$Sb_{0.73}As_{0.27}$	2.592
Sb7	$Sb_{1.00}$	2.617	$Sb_{1.00}$	2.606
As8	$Sb_{0.53}As_{0.47}$	2.395	$As_{0.63}Sb_{0.37}$	2.363
Sb9a/Pb9b	$Sb_{0.81}Pb_{0.19}$	2.646/2.975	$Sb_{0.96}Pb_{0.04}$	2.712/2.967
Sb10a/Ag10b	$Sb_{0.71}Ag_{0.29}$	2.728/2.847	$Sb_{0.60}Ag_{0.40}$	2.713/2.826

s.o.f. – site occupation factor.

https://doi.org/10.1180/minmag.2016.080.068 Published online by Cambridge University Press

TABLE 7. Proposed site occupancies at mixed (Tl/Pb) sites.

Site	B & O	B *et al.*	Proposed
Type boscardinite			
Orlandi *et al.* (2012) – ΣTl_{EPMA} = 1.23 (# 4977)			
(Tl,Pb)1	$Tl_{0.81}Pb_{0.19}$	$Tl_{1.00}$	$Tl_{0.80}Pb_{0.20}$
(Pb,Tl)2a	$Pb_{0.27}Tl_{0.11}$	$Pb_{0.22}Tl_{0.16}$	$Pb_{0.27}Tl_{0.11}$
(Pb,Tl)2b	$Pb_{0.48}Tl_{0.12}$	$Pb_{0.42}Tl_{0.20}$	$Pb_{0.50}Tl_{0.12}$
(Pb,Tl)3	$Pb_{0.79}Tl_{0.21}$	$Pb_{0.70}Tl_{0.30}$	$Pb_{0.80}Tl_{0.20}$
ΣTl	1.25	1.66	1.23
(Tl,As)-enriched boscardinite			
This work – ΣTl_{EPMA} = 1.52 (# 1)			
Tl1	$Tl_{0.80}Pb_{0.20}$	$Tl_{0.99}Pb_{0.01}$	$Tl_{0.90}Pb_{0.10}$
Tl2a	$Pb_{0.24}Tl_{0.17}$	$Tl_{0.22}Pb_{0.19}$	$Tl_{0.23}Pb_{0.18}$
Tl2b	$Tl_{0.30}Pb_{0.29}$	$Tl_{0.39}Pb_{0.20}$	$Tl_{0.38}Pb_{0.21}$
ΣTl	1.27	1.60	1.51

Site occupancies calculated according to the bond-valence parameter $R_{Tl,S}$ proposed by Brese and O'Keeffe (1991) ['B & O'] and by Biagioni *et al.* (2014*a*) ['B *et al.*'].

and Sb sub-sites. The low BVS at the Pb3 site in type boscardinite could also be the result of an average position of this site. If so, the high Tl content obtained by using the BVS parameter of 2.55 Å for type boscardinite (1.66 Tl apfu) could be explained. Consequently, neglecting the contribution of the (Pb,Tl)3 site, the ΣTl (in apfu) would be 1.04 and 1.36 according to the bond-valence parameter of Brese and O'Keeffe (1991) and Biagioni *et al.* (2014*a*), respectively. This would confirm that the use of the $R_{Tl,S}$ bond-valence parameter by Brese and O'Keeffe (1991) for mixed (Tl,Pb) results in an overestimation of Pb, as discussed by Biagioni *et al.* (2015) for chabournéite and protochabournéite.

The other sites occurring in the dufrénoysite and sartorite type layers do not show significant changes in their coordination environments; the only difference is related to the shortest average <*Me*–S> distances in mixed (Sb/As) sites resulting from the strong enrichment in As of the crystal studied. Finally, the difference between the average bond distance at the Sb9a position (see Table 6) has to be related to the cut-off distance used for such a calculation; indeed, by using only <Me^{3+}–S> distances shorter than 3.0 Å, Sb at the Sb9a is bonded to four S atoms in type boscardinite (the fifth being at 3.02 Å), whereas in (Tl,As)-enriched boscardinite there are five S closer than 3.0 Å to Sb9a (the fifth at 2.98 Å). Considering only the four shortest distances, the average <Sb9a–S> distances are 2.646 Å in both the crystal structures.

Polymerization of (Sb,As) sites

Within the sartorite and dufrénoysite type layers, the examination of the shortest (= the strongest, i.e. distance < 2.70 Å, following the approach of Moëlo *et al.*, 2012) Me^{3+}–S bonds allows the description of the organization of Me^{3+} sites into finite $Me^{3+}_m S_n$ chain fragments ('polymers' hereafter). By using such a cut-off distance, Sb and As atoms usually show the classic triangular pyramidal coordination. The exception is represented by the central part of the dufrénoysite layer with split (Sb/Ag) and (Sb/Pb) positions, having only two short distances (Sb7) or a single one (Sb10a). Such exceptions are related to uncertainties in these mixed and split positions or to possible mean positions (Sb10a – see below).

The sartorite layer is characterized by a central 'polymer' $[Sb_4(As_{0.87}Sb_{0.13})_2]_{\Sigma 6}S_{10}$, with two lateral $(As_{0.60}Sb_{0.40})S_3$ groups (Fig. 2). In type boscardinite, the lateral groups are Sb-dominant, i.e. $(Sb_{0.71}As_{0.29})S_3$. Such a polymeric organization has also been described in the other thallium-lead sulfosalt from Monte Arsiccio, protochabournéite (Orlandi *et al.*, 2013), with the 'polymer' $[Sb_4(Sb,As)_2]_{\Sigma 6}S_{10}$ flanked by two isolated $(Sb,As)S_3$ pyramidal groups. The same configuration occurs in chabournéite from Jas Roux (Biagioni *et al.*, 2015), but the higher As/(As + Sb)$_{at.}$ ratio with respect to protochabournéite favours the As-to-Sb substitution at the isolated trigonal pyramids, as observed in (Tl,As)-enriched boscardinite with respect to type boscardinite.

In the dufrénoysite layer, the size of the polymer is determined by the presence or absence of Sb at the mixed split (Sb/Pb)9 and (Sb/Ag)10 positions. The same configuration has been reported in other lead sulfosalts: senandorite (Sawada *et al.*, 1987), sartorite (Berlepsch *et al.*, 2003), the pair sterryite–parasterryite (Moëlo *et al.*, 2012) and carducciite (Biagioni *et al.*, 2014*c*).

The most probable polymerization scheme in the dufrénoysite layer is represented in Fig. 3, according to the following choices: (1) due to its very low s.o.f. (0.04), Pb9b has been neglected; (2) a half occupancy of Ag and Sb on the (Sb/Ag)10 position has been assumed. For local valence equilibrium, when Ag is present on one position, Sb is present on the neighbouring equivalent position; (3) Sb10a has only one *Me*–S distance (with S10) shorter than 2.70 Å; however, there are three other distances only a little longer, ranging between 2.72 and 2.75 Å (a second bond with S10, and two other bonds with S5 and S6). This Sb10a position is clearly a mean position between two sub-positions (not represented in Fig. 3), Sb10a' bound to S5 and

https://doi.org/10.1180/minmag.2016.080.068 Published online by Cambridge University Press

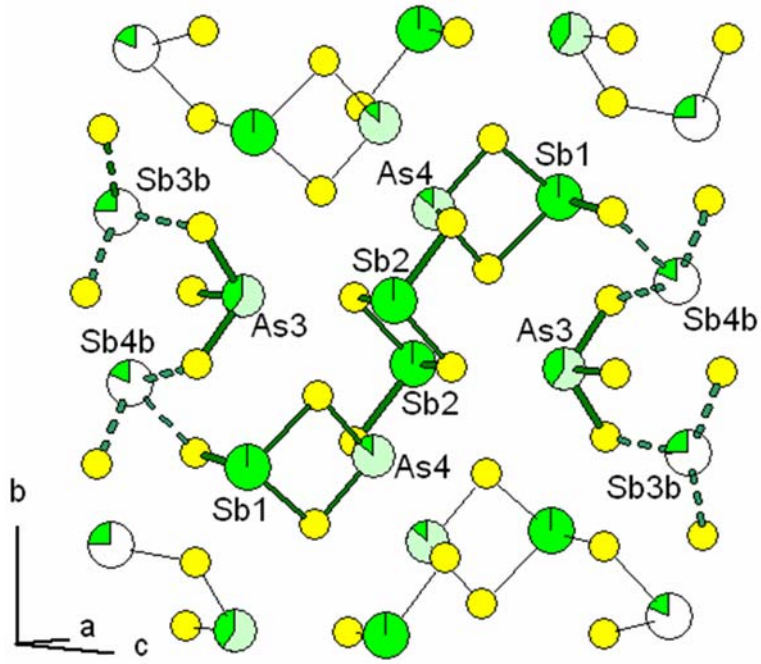

FIG. 2. Polymerization within the sartorite layer of (Tl,As)-enriched boscardinite.

the two S10 and Sb10a'' bound to S6 and also to the two S10.

On this basis, one obtains the combination of two polymers, $Sb_3(Sb,As)_2(As,Sb)S_{11}$ and $Sb_2(Sb,As)_2(As,Sb)S_9$.

Within a dufrénoysite layer, polymers of adjacent identical ribbons (R1 and R2) along **a** are also connected through (As,Sb)5 (R1) and Sb9a (R2) via S14 (R1). Moreover, when present, interlayer Sb3b and Sb4b (Figs 2 and 3) constitute bridging cations between the polymers of the two layer types. The resulting polymerization within the whole structure is thus more complex and variable.

Discussion

Structural formula of (Tl,As)-enriched boscardinite

The formula of the (Tl,As)-enriched boscardinite obtained through the crystal structure refinement is $Ag_{0.40}Tl_{1.51}Pb_{2.10}(Sb_{7.13}As_{2.86})_{\Sigma 9.99}S_{18}$ ($Z = 2$), with the relative error on the valence equilibrium $Ev(\%) = +0.22$. With respect to the chemical analysis, the $As/(As + Sb)_{at.}$ ratio is slightly smaller, i.e. 0.29 *vs.* 0.31.

This structural formula can be reduced to a stoichiometric one by considering the structural fragment where the mixed or split sites having different valence states are located (see fig. 9 in Orlandi *et al.*, 2012). The composition resulting from these sites is $Ag_{0.40}Tl_{1.51}Pb_{2.10}Sb_{1.99}$, and the total valence is 12.08, ideally 12. The sites on the zig-zag layers correspond to $Tl_{1.51}Pb_{2.06}$, which can be simplified as $Tl_{1.5}Pb_2$. The two split (Sb,Pb) and (Sb,Ag) sites correspond to $Ag_{0.40}Sb_{1.56}Pb_{0.04}$. Through the substitution $Ag^+ + Sb^{3+} = 2Pb^{2+}$, it becomes $Sb_{1.16}Pb_{0.84}$, which can be simplified as SbPb. Thus, the simplified Ag-free formula of (Tl,As)-enriched boscardinite is $Tl_{1.5}Pb_3(Sb_{6.5}As_3)_{\Sigma 9.5}S_{18}$.

Nevertheless, it should be emphasized that Ag is always a minor component in boscardinite. Thus, the composition of the two split (Sb/Pb) and (Sb/Ag) sites could alternatively be simplified as $Ag_{0.5}Sb_{1.5}$. If so, the simplified formula of (Tl,As)-enriched boscardinite could be $Ag_{0.5}Tl_{1.5}Pb_2(Sb_7As_3)_{\Sigma 10}S_{18}$ ($Z = 2$). Thus, in order to enhance the possible specific crystal chemical role of Ag, the stoichiometric formula $AgTl_3Pb_4(Sb_{14}As_6)_{\Sigma 20}S_{36}$ ($Z = 1$) would be more convenient. Applying the same consideration to type boscardinite, the Ag-rich derived formula $AgTl_2Pb_6(Sb_{15}As_4)_{\Sigma 19}S_{36}$ is obtained.

https://doi.org/10.1180/minmag.2016.080.068 Published online by Cambridge University Press

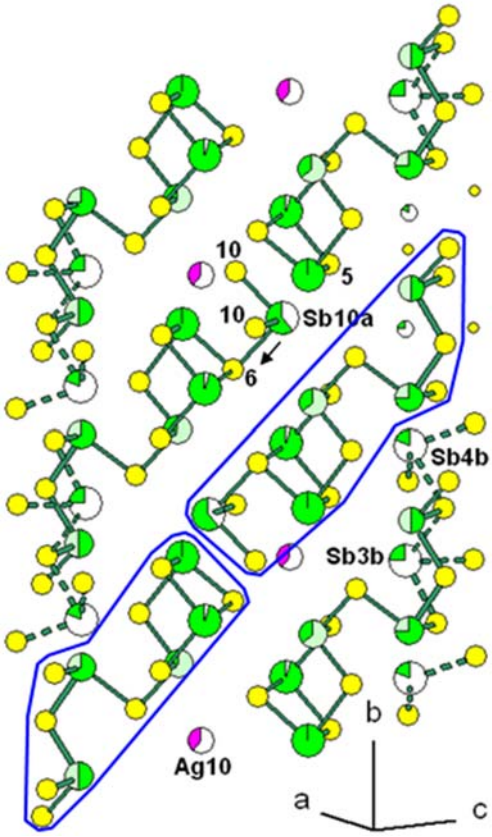

FIG. 3. Main polymerization scheme (proposal) within the dufrénoysite layer of (Tl,As)-rich boscardinite (Pb9b absent, Sb10a alternation with Ag10b). Blue lines enclose the two polymers $Sb_3(Sb,As)_2(As,Sb)S_{11}$ and $Sb_2(Sb,As)_2(As,Sb)S_9$. Black arrow: shift of Sb10a towards S6 (a shift towards S5 is equiprobable).

On the basis of the generalized formula proposed by Orlandi *et al.* (2012), $Ag_xTl_{1+y}Pb_{4-2x-2y}(Sb_{7+x+y+z}As_{2-z})_{\Sigma 9+x+y}S_{18}$, (Tl,As)-enriched boscardinite (sample #408) has $x \approx 0.40$, $y \approx 0.50$ and $z \approx -0.90$. Sample #2 corresponds to $x \approx 0.35$, $y \approx 0.40$ and $z \approx -0.80$.

The (Tl,As)-enriched boscardinite shows a low amount of Hg. This feature agrees with the Hg-rich nature of the sulfosalt assemblages from Monte Arsiccio (Biagioni *et al.*, 2013) and the association of samples #408 and #2 with routhierite, $CuHg_2TlAs_2S_6$ and cinnabar, HgS, respectively. Mercury could be hosted at the partially occupied Ag10b site, in agreement with the Hg^{2+} to Ag^{+} substitution observed in other lead sulfosalts (e.g. rouxelite – Orlandi *et al.*, 2005; Biagioni *et al.*, 2014*b*).

Comparison with type boscardinite

As stated in the introduction, these new occurrences of boscardinite are definitely enriched in As (as well as Tl) with respect to the type specimen. The $As/(As + Sb)_{at.}$ ratio is 0.31 (sample #408), to be compared with 0.21–0.24 of type specimen. This explains the volume decrease of (Tl,As)-enriched boscardinite (≈–0.8%). Nevertheless, while the *b* parameter decreases (–1.15%), *a* and *c* slightly increase (0.11 and 0.27%, respectively). Indeed, two competing mechanisms take place: a volume decrease, related to the As-Sb substitution, and a volume increase due to the Tl-Pb replacement.

In the crystal structure of (Tl,As)-enriched boscardinite, As exceeds Sb in three sites: As3, As4 and As8. The Sb5 site has a s.o.f. close to $Sb_{0.5}As_{0.5}$. In type boscardinite, only one site (As4) is an As-dominant site. The main As-enrichment is observed in the sartorite type layer relative to the dufrénoysite type one. In the former layer, the $As/(As + Sb)_{at.}$ ratio is 0.368, to be compared with 0.26 in type boscardinite. In the latter, the ratio is 0.250, to be compared with 0.125 in type specimen. The predominantly As- and Sb-occupied sites are distributed within the layers in a chess board pattern, similar to those observed in other members of the sartorite homologous series (e.g. guettardite – Makovicky *et al.*, 2012; twinnite – Makovicky and Topa, 2012; barikaite – Makovicky and Topa, 2013). This As-*vs.*-Sb partitioning appears as the main factor controlling the ~8 Å superstructure, that minimizes the steric distortions between As- and Sb-rich sites.

The Tl-rich sites are bound closely to the polymeric organization of (Sb/As) sites of the sartorite type layer, i.e. of the As-rich layer; the reverse is true for Pb-rich sites which are preferentially bound to the dufrénoysite-type layer. On this basis, the structural formula can be cut into two sub-parts (formula refers to ribbons): (1) sartorite-type layer, with Tl-rich sites: $[(Tl_{3.02}Pb_{0.98})_{\Sigma 4}(Sb_{5.06}As_{2.94})_{\Sigma 8}S_{16}]^{-3.02}$; and (2) dufrénoysite-type layer, with Pb-rich sites: $[(Pb_{3.136}Sb_{0.864})_{\Sigma 4}(Ag_{0.80}Pb_{0.088}Sb_{8.332}As_{2.78})_{\Sigma 12}S_{20}]^{+3.18}$.

Contrary to type boscardinite, this new occurrence displays Pb-rich sites containing some Sb, with no Tl (even if the Tl at the Pb3 site in type boscardinite could be due to a misinterpretation – see above).

https://doi.org/10.1180/minmag.2016.080.068 Published online by Cambridge University Press

(Tl,As)-enriched boscardinite: variety or a new mineral species?

Boscardinite, ideally $TlPb_4(Sb_7As_2)_{\Sigma 9}S_{18}$, and (Tl, As)-enriched boscardinite, ideally $Tl_{1.5}Pb_3(Sb_{6.5}As_3)_{\Sigma 9.5}S_{18}$, significantly differ both chemically and structurally. Clearly, these differences are remarkable from a crystal-chemical point of view, giving new insights on the As-to-Sb partitioning in the members of the sartorite homologous series. Nevertheless, these differences are not sufficient to propose a new mineral species.

Two kinds of substitution take place: (1) the isovalent $Sb^{3+} = As^{3+}$ substitution; and (2) the heterovalent $Tl^{+} + Me^{3+} = 2Pb^{2+}$. Substitution (1) involves the occurrence of sites having different As- or Sb-dominance, but with $As_{tot} < Sb_{tot}$ as in type boscardinite. In boscardinite and its (Tl,As)-enriched analogue, the As-to-Sb substitution causes no differences in crystallographic characteristics between the two phases, i.e. no different symmetries, or space groups, or superstructures. Substitution (2) is demonstrated, taking into account the Tl substitution percentage, as boscardinite and its (Tl,As)-enriched isotype are intermediate members between the unsubstituted $Pb_6(Sb,As)_8S_{18}$ and the fully substituted Tl end-member $Tl_3(Sb,As)_{11}S_{18}$. The Tl subst.% values, calculated following the procedure described by Makovicky and Topa (2015), range from ~37% (sample #4989 of type boscardinite) and ~50% of sample #408 of (Tl,As)-enriched boscardinite. As stressed in the previous paragraph, Ag seems to be a minor but characteristic component of boscardinite. The Ag subst.% values in split (Sb10a, Ag10b) range between ~30% (sample #4989) and 43% (sample #408).

From these calculations, it appears that (Tl,As)-enriched boscardinite does not significantly exceed the 50% substitution of either Tl or Ag (and obviously of As) and consequently it should be considered only as a (Tl,As)-enriched variety of boscardinite. Actually, sample #408 has a Tl subst.% slightly higher than 50 (i.e. 50.33%). But it should be noted that, even if the experimental error is ignored, the known compositional range of boscardinite ranges between 30 and 50%. Thus, the rule proposed by Nickel (1992) could be applied: '*If the known compositions embrace the 50% mark but do not appear to extend to either end-member* […], *only one name should be applied to the compositional range*'. In conclusion, (Tl,As)-enriched boscardinite can be considered simply as a variety of boscardinite.

What is the exact definition of boscardinite?

Initially, members of the sartorite homologous series were defined as lead-arsenic sulfosalts. Later, since the first description of antimonian baumhauerite from Madoc, Ontario, Canada (Jambor, 1967*a*,*b*), Sb-containing analogues were described. Boscardinite was the first N = 3.5 homologue having Sb > As. Actually, it is the Tl-Sb analogue of baumhauerite, ideally $Pb_6As_8S_{18}$. Recently, a new N = 3.5 homologue characterized by the occurrence of Sb and As has been described: bernarlottiite, $Pb_6(As_5Sb_3)S_{18}$ (Orlandi *et al.*, 2014).

Type boscardinite was defined as $TlPb_4(Sb_7As_2)_{\Sigma 9}S_{18}$. Its chemical variability points to even higher Tl and As contents, up to $Tl_{1.5}Pb_3(Sb_{6.5}As_3)_{\Sigma 9.5}S_{18}$. Increasing the Tl content, one could obtain the compound $Tl_2Pb_2(Sb,As)_{10}S_{18}$, i.e. $TlPb(Sb,As)_5S_9$. This chemical formula corresponds to the Sb analogue of hutchinsonite, $TlPbAs_5S_9$, a mineral showing a different structural arrangement, belonging to the hutchinsonite merotypic series (Makovicky, 1997). Actually, the role of Ag in the N = 3.5 homologue structure is not known; it could hypothetically stabilize boscardinite up to higher Tl content. Silver content similar to those occurring in boscardinite seems to control the formation and to give rise to superstructure reflections in 'baumhauerite-2*a*' (Laroussi *et al.*, 1989; Pring *et al.*, 1990; Pring and Graeser, 1994), recently redefined as argento-baumhauerite (Hålenius *et al.*, 2015). On the contrary, type boscardinite, studied using synchrotron radiation, shows no superstructure reflections. However, the hypothesis of the possible existence of domains of 'boscardinite-2*a*' within a boscardinite matrix could not be discarded. Further study is mandatory.

The comparison of boscardinite with other members of the sartorite homologous series is interesting. If two unit formulas of sartorite, ideally $PbAs_2S_4$, are added to two units of the ideal formula of philrothite, $TlAs_3S_5$ (Bindi *et al.*, 2014), one gets:

$$2 \times PbAs_2S_4 + 2 \times TlAs_3S_5 = Tl_2Pb_2As_{10}S_{18},$$

corresponding to an As-analogue of (Tl,As)-enriched boscardinite, with one Pb replaced by (0.5Tl + 0.5As).

Boscardinite is currently defined as the Tl-Sb analogue of baumhauerite, with idealized formula $Tl_{1+x}Pb_{4-2x}(Sb,As)_{9+x}S_{18}$ $(0 < x < 0.5)$. If $x < 0$, then a new potential Sb-baumhauerite is obtained.

https://doi.org/10.1180/minmag.2016.080.068 Published online by Cambridge University Press

Tl contents higher than 1.5 apfu ($x > 0.5$) should enlarge the compositional field of boscardinite, leading potentially to a new chemical pole.

Thallium-lead sulfosalts from the Monte Arsiccio mine

Boscardinite, as well as protochabournéite, are the two thallium-lead sulfosalts having their type locality at the Monte Arsiccio mine, Apuan Alps, Tuscany, Italy. This small baryte + pyrite + iron oxides abandoned mine has recently become a reference locality for the study of thallium sulfosalts. In addition to thallium sulfosalts *sensu stricto*, Tl-bearing varieties of rouxelite, robinsonite, chovanite and twinnite have been identified (e.g. Biagioni *et al.*, 2014*b*). Three kinds of sulfosalt occurrences have been identified: (1) Type 1: microcrystalline baryte + pyrite ore bodies, at the contact between schist and dolostone; (2) Type 2: pyrite-rich dolostone, near the contact with the schist; and (3) Type 3: carbonate (usually dolomite) ± baryte ± quartz veins embedded in the dolostone.

The complexity of the ore geochemistry at Monte Arsiccio and these different kinds of sulfosalt occurrences are reflected in the crystal-chemistry of the minerals studied. Biagioni *et al.* (2014*a*) discussed the chemical variability of the pair arsiccioite-routhierite as a function of their kind of occurrence, showing an increase in the $As/(As + Sb)_{at.}$ ratio passing from the pyrite-rich dolostone to the microcrystalline baryte + pyrite ore bodies.

New chemical data collected on boscardinite and protochabournéite seem to confirm such a significant chemical variability in sulfosalts. The Pb/(Pb + 2Tl) *vs.* As/(As + Sb) atomic ratio in the chabournéite series and boscardinite is shown in Fig. 4. In addition to the two new chemical analyses of boscardinite reported above, three other samples were previously characterized chemically, representative of Type 2 and Type 1 occurrences (unpublished data). Two additional samples from Type 2 occurrence (#371 and #409) have chemical composition (on the basis of $\Sigma Me = 14$ apfu) $Ag_{0.40}Tl_{1.20}Pb_{2.75}Hg_{0.01}(Sb_{7.00}As_{2.64})_{\Sigma 9.64}S_{18.20}$ and $Ag_{0.34}Tl_{1.35}Pb_{2.59}Hg_{0.02}(Sb_{6.88}As_{2.81})_{\Sigma 9.69}S_{18.24}$, with $As/(As + Sb)_{at.}$ ratio of 0.274 and 0.290, respectively. Boscardinite from Type 1 occurrence (sample #404) is richer in As than sample #408, having the composition $Ag_{0.38}Tl_{1.42}Pb_{2.45}Hg_{0.02}(Sb_{6.52}As_{3.21})_{\Sigma 9.73}S_{18.18}$, with $As/(As + Sb)_{at.}$ ratio of 0.330. Consequently,

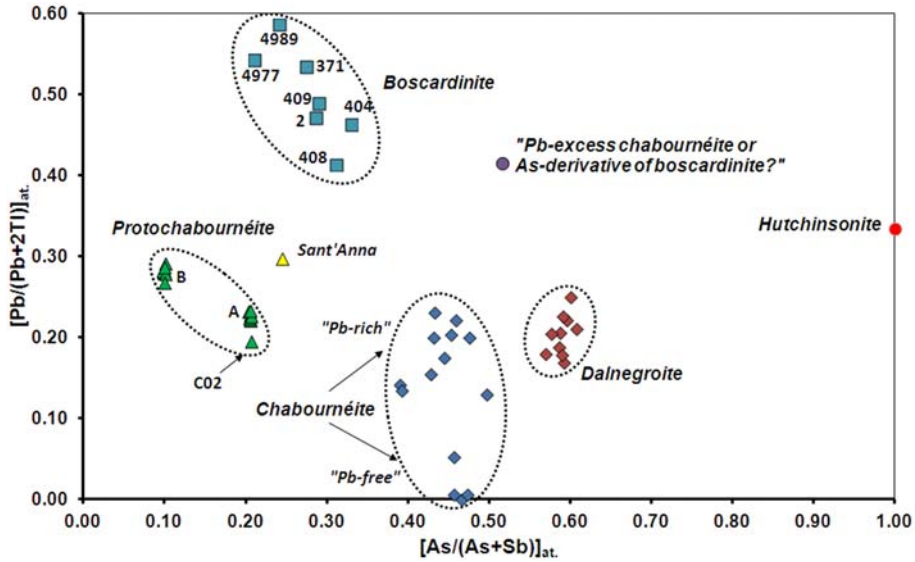

FIG. 4. As/(As + Sb) *vs.* Pb/(Pb + 2Tl) atomic ratio in the chabournéite series and in boscardinite. Lozenges: chabournéite (data after Mantienne, 1974; Johan *et al.*, 1981; Shimizu *et al.*, 1999; Biagioni *et al.*, 2015; D. Harris, pers. comm., 1989) and dalnegroite (Nestola *et al.*, 2009). Triangles: protochabournéite (A and B correspond to analyses given in Orlandi *et al.*, 2013). Square: boscardinite (4977 and 4989 correspond to analyses of type boscardinite given in Orlandi *et al.*, 2012; the remaining analyses are discussed in the text). Circles: Pb-excess chabournéite derivative or As-boscardinite derivative (data after Johan *et al.*, 1981) and ideal chemical composition of hutchinsonite, $TlPbAs_5S_9$.

https://doi.org/10.1180/minmag.2016.080.068 Published online by Cambridge University Press

boscardinite seems to show an increase in Tl and As passing from Type 3 occurrence (Type boscardinite, samples #4977 and #4989 in Fig. 4) to Type 1 occurrence (sample #404). In addition, (Tl,As)-enriched boscardinite has been identified in the Sant'Anna level, in association with a 'protochabournéite-like' mineral. It is interesting to observe that the $Pb/(Pb + 2Tl)_{at.}$ ratio of (Tl,As)-enriched boscardinite is similar to the 'Pb-excess chabournéite derivative' reported from Abuta, Japan, by Johan *et al.* (1981). Owing to the absence of structural data on this latter compound, its relationships with boscardinite are not known but it could also correspond to an 'As-rich derivative of boscardinite'.

Protochabournéite, originally described from Type 2 and 3 occurrences, was later identified in Type 1 occurrence (sample C02 in Fig. 4). Its chemical analysis gave the following result [same analytical conditions described for (Tl,As)-enriched boscardinite] (in wt.%, mean of four spot analyses): Tl 18.06 (11), Pb 8.81(13), Sb 41.93(53), As 6.73(18), S 23.57 (19), sum 99.10(96). Its chemical formula, on the basis of $\Sigma Me = 13$ apfu, is $Tl_{2.03(1)}Pb_{0.98(1)}Sb_{7.92(4)}As_{2.07(5)}S_{16.91(7)}$, $Ev(\%) = +0.4$. This new occurrence is similar to analysis of sample A in Orlandi *et al.* (2013), with a slightly higher Tl content. On the contrary, the 'protochabournéite-like' mineral observed intimately associated with (Tl,As)-enriched boscardinite from the Sant'Anna level has some chemical peculiarities, showing high $Pb/(Pb + 2Tl)$ and $As/(As + Sb)_{at.}$ ratios with respect to type protochabournéite. Its chemical analyses (average of three spot analyses) gave (in wt.%): Tl 15.85(6), Pb 13.52(43), Hg 0.04(3), Sb 38.84(22), As 7.76 (22), S 23.70(25), Cl 0.05(1), sum 99.77(113). The chemical formula is $Tl_{1.78(2)}Pb_{1.50(3)}Hg_{0.01(1)}Sb_{7.33(5)}As_{2.38(4)}S_{16.99(6)}Cl_{0.03(1)}$, $Ev(\%) = -0.2$. An X-ray diffraction study is necessary to confirm its identity with protochabournéite.

Conclusion

The thallium-rich sulfosalt assemblage from Monte Arsiccio represents an interesting field of research for the study of sulfosalt crystal-chemistry owing to its complex geochemistry, associating Tl with Pb, Sb, As, Ag, Hg and Cu. The occurrence of a (Tl, As)-rich variety of boscardinite refines the knowledge about the N = 3.5 homologues of the sartorite series, providing new data on the partitioning of As and Sb within these compounds. The upper limit in Tl content in N = 3.5 homologues, as well as the role of Ag, should be clarified by further studies.

The chemical variability observed in thallium-lead sulfosalts confirms the exceptional mineralogical complexity of the baryte-pyrite-iron oxides ore deposits from the Apuan Alps, where small changes in the ore geochemistry control the crystallization of a great variety of different sulfosalts.

Acknowledgements

Electron microprobe analyses were performed with the help of J. Langlade (CNRS engineer, 'Microsonde Ouest' laboratory, IFREMER, Plouzané, France). This research received support by MIUR through project SIR 2014 'THALMIGEN – Thallium: Mineralogy, Geochemistry, and Environmental Hazards', granted to CB. The manuscript benefited from the comments of Emil Makovicky and an anonymous reviewer.

REFERENCES

Berlepsch, P., Armbruster, T. and Topa, D. (2002) Structural and chemical variations in rathite, $Pb_8Pb_{4-x}(Tl_2As_2)_x(Ag_2As_2)As_{16}S_{40}$: modulations of a parent structure. *Zeitschrift für Mineralogie*, **217**, 581–590.

Berlepsch, P., Armbruster, T., Makovicky, E. and Topa, D. (2003) Another step toward understanding the true nature of sartorite: determination and refinement of a ninefold superstructure. *American Mineralogist*, **88**, 450–461.

Biagioni, C., D'Orazio, M., Vezzoni, S., Dini, A. and Orlandi, P. (2013) Mobilization of Tl-Hg-As-Sb-(Ag,Cu)-Pb sulfosalt melts during low-grade metamorphism in the Alpi Apuane (Tuscany, Italy). *Geology*, **41**, 747–751.

Biagioni, C., Bonaccorsi, E., Moëlo, Y., Orlandi, P., Bindi, L., D'Orazio, M. and Vezzoni, S. (2014*a*) Mercury-arsenic sulfosalts from the Apuan Alps (Tuscany, Italy). II. Arsiccioite, $AgHg_2TlAs_2S_6$, a new mineral from the Monte Arsiccio mine: occurrence, crystal structure and crystal chemistry of the routhierite isotypic series. *Mineralogical Magazine*, **78**, 101–117.

Biagioni, C., Moëlo, Y. and Orlandi, P. (2014*b*) Lead-antimony sulfosalts from Tuscany (Italy). XV. (Tl-Ag)-bearing rouxelite from Monte Arsiccio mine: occurrence and crystal structure. *Mineralogical Magazine*, **78**, 651–661.

Biagioni, C., Orlandi, P., Moëlo, Y. and Bindi, L. (2014*c*) Lead-antimony sulfosalts from Tuscany (Italy). XVI. Carducciite, $(AgSb)Pb_6(As,Sb)_8S_{20}$, a new Sb-rich derivative of rathite from the Pollone mine, Valdicastello Carducci: occurrence and crystal structure. *Mineralogical Magazine*, **78**, 1775–1793.

Biagioni, C., Moëlo, Y., Favreau, G., Bourgoin, V. and Boulliard, J.-C. (2015) Structure of Pb-rich chabournéite from Jas Roux, France. *Acta Crystallographica*, **B71**, 81–88.

https://doi.org/10.1180/minmag.2016.080.068 Published online by Cambridge University Press

Bindi, L., Nestola, F., Makovicky, E., Guastoni, A. and De Battisti, L. (2014) Tl-bearing sulfosalt from the Lengenbach quarry, Binn Valley, Switzerland: Philrothite, $TlAs_3S_5$. *Mineralogical Magazine*, **78**, 1–9.

Brese, N.E. and O'Keeffe, M. (1991) Bond-valence parameters for solids. *Acta Crystallographica*, **B47**, 192–197.

Bruker AXS Inc. (2004) *APEX 2*. Bruker Advanced X-ray Solutions, Madison, Wisconsin, USA.

Hålenius, U., Hatert, F., Pasero, M. and Mills, S.J. (2015) IMA Commission on New Minerals, Nomenclature and Classification (CNMNC) Newsletter 25. *Mineralogical Magazine*, **79**, 529–535.

Jambor, J.L. (1967*a*) New lead sulfantimonides from Madoc, Ontario – Part 1. *The Canadian Mineralogist*, **9**, 7–24.

Jambor, J.L. (1967*b*) New lead sulfantimonides from Madoc, Ontario. Part 2 – Mineral descriptions. *The Canadian Mineralogist*, **9**, 191–213.

Johan, Z., Mantienne, J. and Picot, P. (1981) La chabournéite, un nouveau minéral thallifère. *Bulletin de Minéralogie*, **104**, 10–15.

Laroussi, A., Moëlo, Y., Ohnenstetter, D. and Ginderow, D. (1989) Argent et thallium dans les sulfosels de la série de la sartorite (gisement de Lengenbach, vallée de Binn, Suisse). *Comptes Rendus de l'Académie des Sciences Paris*, **308**, 927–933.

Makovicky, E. (1985) The building principles and classification of sulphosalts based on the SnS archetype. *Fortschritte der Mineralogie*, **63**, 45–89.

Makovicky, E. (1997) Modular crystal chemistry of sulphosalts and other complex sulphides. Pp. 237–271 in: *Modular Aspects of Minerals* (S. Merlino, editor). European Mineralogical Union, Notes in Mineralogy, **1**. Eötvös University Press, Budapest.

Makovicky, E. and Topa, D. (2012) Twinnite, $Pb_{0.8}Tl_{0.1}Sb_{1.3}As_{0.8}S_4$, the OD character and the question of its polytypism. *Zeitschrift für Kristallographie*, **227**, 468–475.

Makovicky, E. and Topa, D. (2013) The crystal structure of barikaite. *Mineralogical Magazine*, **77**, 3093–3104.

Makovicky, E. and Topa, D. (2015) Crystal chemical formula for sartorite homologues. *Mineralogical Magazine*, **79**, 25–31.

Makovicky, E., Topa, D., Taijedin, H., Rastad, E. and Yaghubpur, A. (2012) The crystal structure of guettardite, $PbAsSbS_4$, and the twinnite-guettardite problem. *The Canadian Mineralogist*, **50**, 253–265.

Mantienne, J. (1974) *La minéralisation thallifere de Jas Roux (Hautes-Alpes)*. Unpublished thesis, Université de Paris, 146 pp.

Moëlo, Y., Guillot-Deudon, C., Evain, M., Orlandi, P. and Biagioni, C. (2012) Comparative modular analysis of two complex sulfosalt structures: sterryite, $Cu(Ag,Cu)_3Pb_{19}(Sb,As)_{22}(As–As)S_{56}$, and parasterryite, $Ag_4Pb_{20}(Sb,As)_{24}S_{58}$. *Acta Crystallographica*, **B68**, 480–492.

Nestola, F., Guastoni, A., Bindi, L. and Secco, L. (2009) Dalnegroite, $Tl_{5-x}Pb_{2x}(As,Sb)_{21-x}S_{34}$, a new thallium sulphosalt from Lengenbach quarry, Binntal, Switzerland. *Mineralogical Magazine*, **73**, 1027–1032.

Nickel, E.H. (1992) Nomenclature for mineral solid solutions. *American Mineralogist*, **77**, 660–662.

Orlandi, P., Moëlo, Y., Meerschaut, A., Palvadeau, P. and Léone, P. (2005) Lead-antimony sulfosalts from Tuscany (Italy). VIII. Rouxelite, $Cu_2HgPb_{22}Sb_{28}S_{64}(O,S)_2$, a new sulfosalt from Buca della Vena mine, Apuan Alps: definition and crystal structure. *The Canadian Mineralogist*, **43**, 919–933.

Orlandi, P., Biagioni, C., Bonaccorsi, E., Moëlo, Y. and Paar, W. (2012) Lead-antimony sulfosalts from Tuscany (Italy). XII. Boscardinite, $TlPb_4(Sb_7As_2)_{\Sigma 9}S_{18}$, a new mineral species from the Monte Arsiccio mine: occurrence and crystal structure. *The Canadian Mineralogist*, **50**, 235–251.

Orlandi, P., Biagioni, C., Moëlo, Y., Bonaccorsi, E. and Paar, W. (2013) Lead-antimony sulfosalts from Tuscany (Italy). XIII. Protochabournéite, $\sim Tl_2Pb(Sb_{9-8}As_{1-2})_{\Sigma 10}S_{17}$, from the Monte Arsiccio mine: occurrence, crystal structure and relationship with chabournéite. *The Canadian Mineralogist*, **51**, 475–494.

Orlandi, P., Biagioni, C., Bonaccorsi, E., Moëlo, Y. and Paar, W.H. (2014) Bernarlottiite, IMA 2013-133. CNMNC Newsletter No. 20, June 2014, page 553. *Mineralogical Magazine*, **78**, 549–558.

Pring, A. and Graeser, S. (1994) Polytypism in baumhauerite. *American Mineralogist*, **79**, 302–307.

Pring, A., Birch, W.D., Sewell, D., Graeser, S., Edenharter, A. and Criddle, A. (1990) Baumhauerite-2*a*: A silver-bearing mineral with a baumhauerite-like supercell from Lengenbach, Switzerland. *American Mineralogist*, **75**, 915–922.

Sawada, H., Kawada, I., Hellner, E. and Tokonami, M. (1987) The crystal structure of senandorite (andorite VI): $PbAgSb_3S_6$. *Zeitschrift für Kristallographie*, **180**, 141–150.

Sheldrick, G.M. (2008) A short history of SHELX. *Acta Crystallographica*, **A64**, 112–122.

Shimizu, M., Matsuyama, F. and Shimizu, M. (1999) Hutchinsonite, $TlPb(As,Sb)_5S_9$, Chabournéite, $Tl_2Pb(Sb,As)_{10}S_{17}$, and Unnamed $(Tl,Ag)_2Pb_6(As,Sb)_{16}S_{31}$ from the Toya-Takarada Mine, Hokkaido, Japan – Tl mineralisation in the Kuroko Deposits. *Resource Geology*, **20**, 31–37.

Topa, D., Makovicky, E., Favreau, G., Bourgoin, V., Boulliard, J.-C., Zagler, G. and Putz, H. (2013) Jasrouxite, a new Pb-Ag-As-Sb member of the lillianite homologous series from Jas Roux, Hautes-Alpes, France. *European Journal of Mineralogy*, **25**, 1031–1038.

Wilson, A.J.C. (1992) *International Tables for Crystallography Volume C*. Kluwer, Dordrecht, The Netherlands.

https://doi.org/10.1180/minmag.2016.080.068 Published online by Cambridge University Press